Application and validation of the spherical elementary currents systems technique for deriving ionospheric equivalent currents with the North American and Greenland ground magnetometer arrays

James M. Weygand,[1] Olaf Amm,[2] A. Viljanen,[2] V. Angelopoulos,[1] D. Murr,[3] M. J. Engebretson,[3] H. Gleisner,[4] and I. Mann[5]

Received 4 October 2010; revised 28 December 2010; accepted 7 January 2011; published 4 March 2011.

[1] With data from the Canadian Magnetic Observatory System, Canadian Array for Real time Investigations of Magnetic Activity, Geophysical Institute Magnetometer Array, Greenland, Time History of Events and Macroscale Interactions during Substorms (THEMIS), and Magnetometer Array for Cusp and Cleft Studies ground magnetometer arrays, we applied the state-of-art technique on the basis of spherical elementary currents systems (SECS) developed by Amm and Viljanen (1999) in order to calculate maps of ionospheric equivalent currents over the whole North American auroral region. This study is the first to apply the SECS technique to a large nonrectangular area with widely separated ground magnetometers (~350 km). For this study we will first demonstrate the validity of the technique using synthetic data and then examine equivalent ionospheric currents associated with a Harang discontinuity for a case study on 10 December 2007. The results show in detail the dynamic evolution of the currents over the entire North American ground magnetometer network. Equivalent ionospheric current (EIC) maps inferred at the minimum resolution of the database, in this case 10 s, can thus be analyzed further in conjunction with near-simultaneous images of the THEMIS all-sky imager mosaics and Super Dual Auroral Radar Network radar data. The EIC maps represent a value-added product from the raw magnetometer database and can be used for contextual interpretation as well as help with our understanding of magnetosphere-ionosphere coupling mechanisms using the ground arrays and the THEMIS spacecraft data.

Citation: Weygand, J. M., O. Amm, A. Viljanen, V. Angelopoulos, D. Murr, M. J. Engebretson, H. Gleisner, and I. Mann (2011), Application and validation of the spherical elementary currents systems technique for deriving ionospheric equivalent currents with the North American and Greenland ground magnetometer arrays, *J. Geophys. Res.*, *116*, A03305, doi:10.1029/2010JA016177.

1. Introduction

[2] Equivalent ionospheric currents are a convenient means to study the characteristics of the currents in the ionosphere. A number of methods exist to derive these currents from ground magnetometer stations including the spherical harmonic method [*Chapman and Bartels*, 1940], the spherical cap harmonic method [*Haines*, 1985a, 1985b], and the Fourier method [*Mersmann et al.*, 1979; *Untiedt and Baumjohann*, 1993]. The shortcomings of those methods are that the spectral content of the solution has to be chosen globally, boundary conditions can be important, and aliasing of the spectral solution due to sparsely and unevenly spaced magnetic field measurements sites may occur. A method developed in the late 1990s, which has been regularly applied to the International Monitor for Auroral Geomagnetic Effects (IMAGE) ground magnetometer array, is the spherical elementary current systems (SECS) method [*Amm and Viljanen*, 1999]. The technique defines two elementary current systems: a divergence-free elementary system with currents that flow entirely within the ionosphere and a curl-free system whose divergences represent the field-aligned currents (FACs). The superposition of these two elementary current systems with different weights (scaling factors) can reproduce any vector field on a sphere. If it is known a priori that the vector field is curl-free or divergence-free, then only one set of basic functions is needed, and thus 50% of the free coefficients (those associated with the other current system) can be eliminated. For more details see *Amm and Viljanen* [1999] and references within the study. In this study our

[1]Institute of Geophysics and Planetary Physics, University of California, Los Angeles, California, USA.
[2]Arctic Research Unit, Finnish Meteorological Institute, Helsinki, Finland.
[3]Department of Physics, Augsburg College, Minneapolis, Minnesota, USA.
[4]Danish Meteorological Institute, Copenhagen, Denmark.
[5]Department of Physics, University of Alberta, Edmonton, Alberta, Canada.

0148-0227/11/2010JA016177

Table 1. Ground Magnetometer Arrays and the Number of Stations With Data Potentially Available During 2007 and 2008

Magnetometer Array	Number of Stations
CANMOS	15
CARISMA	8
GIMA	11
Greenland	10
MACCS	5
THEMIS GMAG	43
Total	92

goal is to derive ionospheric equivalent currents, which are by definition divergence free, thus we only use divergence-free elementary systems. Since the basic functions are local, the elementary systems only need to be placed in the area and immediate vicinity of the ground magnetometer networks. The density and geometry of elementary current systems to be determined can be adjusted according to the density and geometry of the ground magnetometer data. No fixed upper and lower wavelength needs to be specified for the modeling, as is needed in harmonic expansions, and no explicit boundary conditions are required. Careful testing of this method has been reported by *Pulkkinen et al.* [2003]. Their results were validated by means of synthetic ionospheric current models and by investigating the goodness of fit between modeled and measured ground magnetometer data. They found that errors on the order of 1% occur when the equivalent ionospheric currents are determined in the region of the ground magnetometers, but farther from the ground magnetometers the error typically increases to 15%.

[3] The motivation of this study is to apply the SECS method to the widely spaced ground magnetometer arrays in North America and Western Greenland. Section 2 will discuss the North American and Western Greenland magnetometer arrays. Section 3 will cover the spatial resolution, selection of grids for the output area, inversion technique and selection of related parameters, and then we will examine a test case with synthetic data. In the last part of section 3, we will apply the technique to a real data case of a Harang discontinuity observed on 10 December 2007. The Harang discontinuity is formed in the ionosphere by an abrupt change in direction of the flow of convecting plasma. Magnetic field lines opened on the dayside move across the polar cap and as they approach the open-closed field line boundary are deflected first toward dawn and then, after becoming closed, move toward dusk. This creates a strong shear in the flow corresponding to a convergent electric field where an upward FAC is observed and a shear in the Hall currents is present.

2. Instrumentation

[4] In order to accurately calculate the SECS over North America and Western Greenland we need a large number of ground magnetometer stations. For this study we have obtained data from six different ground magnetometer arrays: Canadian Magnetic Observatory System (CANMOS), Canadian Array for Real time Investigations of Magnetic Activity (CARISMA), Geophysical Institute Magnetometer Array (GIMA), Greenland, Magnetometer Array for Cusp and Cleft Studies (MACCS) [*Engebretson et al.*, 1995], and Time History of Events and Macroscale Interactions during Substorms ground magnetometers (THEMIS GMAG). Table 1 indicates the number of stations that have data available for the years of 2007 to 2009. Many of the ground magnetometer arrays share some stations. All of the data from GIMA, MACCS, and Greenland stations can be obtained from the THEMIS GMAG online data archive, while CARISMA is also obtained as a link from the above archive to the native database at the University of Alberta. In total we have the potential of obtaining data from 81 different stations at this time. We have not included the Greenland stations on the East coast because these stations are far from rest of the ground magnetometers. Figure 1 displays the distribution of those stations and the key indicates to which array the station belongs.

3. Procedure and Observations

[5] The goal of this study is to adapt the SECS method, which is regularly used in Scandinavia, to the North America and Western Greenland region. Furthermore, we do not include magnetometer data below about 38° geographic latitude because the angle between the magnetic field lines and the ionosphere starts to become large and affects reconstruction of the divergence free current system [e.g., *Amm*, 1998]. The key advantage of applying the SECS technique to the North American data set is the large analysis area offered by the wide coverage of magnetometer stations. With the SECS technique, the analysis area can have any shape, and is not restricted to rectangles or spherical surface area caps as previous studies have used. On the other hand, as compared to the IMAGE magnetometer network, which can yield a spatial resolution of less than 100 km, the North American network in its densest region has a mean equivalent ionospheric current spatial resolution of 320 km (2.9 degrees) in latitude and 380 km (6.9 degrees) in longitude. This resolution is determined from the densest part of the ground magnetometers in Alaska using the GIMA and THEMIS stations. Figure 2 displays the analysis area over which the elementary current amplitudes and the equivalent ionospheric currents are determined (the dot demarcates the

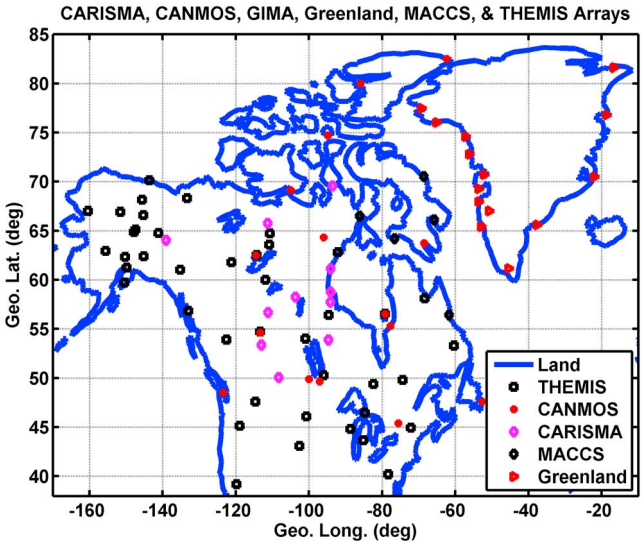

Figure 1. Distribution of ground magnetometer stations within North America and Greenland.

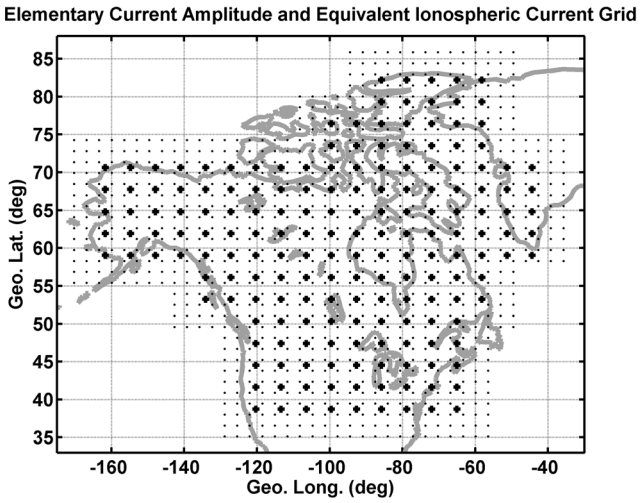

Figure 2. Elementary current amplitudes and equivalent ionospheric current grid. Dots indicate where the SECS amplitudes are calculated, and the plus symbols show the location where the equivalent ionospheric currents are calculated.

elementary current computation grid and the plus symbol the equivalent ionospheric current grid). Note the nonrectangular distribution of the grid, which is different from the rectangular grid normally used for IMAGE network.

3.1. Inversion Technique and Selection of Optimal Parameters

[6] For the calculation of ionospheric equivalent currents from the ground magnetic disturbance field, we used the technique based on SECS [*Amm*, 1997]. The mathematical framework of the technique has been described by *Amm and Viljanen* [1999]. The main purpose of this paper is to demonstrate its applicability to large networks of ground magnetometers as shown in Figure 1, and we only give a brief review of the technique here.

[7] Any vector field on a sphere can be uniquely expanded as a sum of curl-free (*cf*) and divergence-free (*df*) SECS, where the amplitudes (or "scaling factors") of each elementary system are a scalar representation of the vector field. Due to the divergence-free nature of ionospheric equivalent currents [e.g., *Untiedt and Baumjohann*, 1993], only the *df* SECS are needed for their expansion. The magnetic field of each SECS can be analytically calculated both above and below the sphere on which the currents are flowing [see *Amm and Viljanen*, 1999]. Thus the scaling factors of the SECS can be related to the ground magnetic disturbance by the linear relation

$$\overline{\overline{T}} \cdot \overline{I} = \overline{Z}, \tag{1}$$

where $\overline{Z}$ is the vector of measurements, $\overline{I}$ is the searched vector of the SECS scaling factors, and the matrix $\overline{\overline{T}}$ contains the magnetic field effect of a unit SECS placed at each of the positions of the SECS grid (Figure 2), evaluated at each of the observation sites (Figure 1).

[8] Since the problem is typically underdetermined, for the inversion of equation (1) the singular value decomposition (SVD) technique [e.g., *Press et al.*, 1992] is used, which separates out the badly conditioned parts of T. This process is based on a parameter called epsilon that determines the cutoff of the null-space (i.e., the set of all vectors for which the matrix maps to zero) relative to the largest singular value within the SVD technique. In order to obtain optimum results, it is useful to optimize the choice of this epsilon parameter for a given geometry of the problem (i.e., for a given SECS grid and a given network of observations). Since this optimization process is dependent on the geometry and not on the data themselves, it only needs to be performed once for any given magnetometer network. For that optimization, a model SECS distribution is developed, and on top of the ground magnetic field calculated from that model, a random error vector with a magnitude approximately corresponding to the instrumental and baseline uncertainties (in our case estimated to be about 10 nT) is added where the bulk of this uncertainty comes from the baseline estimates at high latitudes. With this "observed" ground magnetic field, the SECS inversion is performed successively for a range of epsilon values. For each of these inversion runs, the integrated difference between the model SECS scaling factors and the resulting scaling factors is calculated (Figure 3). The optimal epsilon value is determined as that value associated with the smallest integrated difference between the model SECS scaling factors and the derived scaling factors. In the case of our geometry as shown in Figures 1 and 2, the resulting optimal epsilon value is ~0.042.

[9] In order to validate the SECS method as applied to the North American arrays a model current system of a Harang discontinuity over North America at 100 km in altitude was developed (Figures 4a and 4b, top). Note that for the model current system *x* axis point northward, the positive z axis points into the page, and the *y* axis completes the right handed coordinate system. From the model the Bx and By magnetic field components were calculated at the location of the magnetometers used in this study. In Figure 4c showing the model−determined horizontal magnetic field vectors at the available stations we see a rotation of the magnetic field

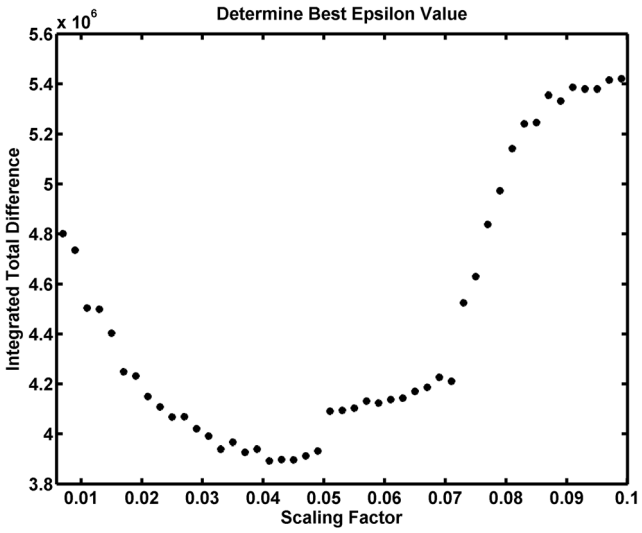

Figure 3. Difference between the integrated model elementary system amplitudes and the integrated derived elementary system amplitudes in the vicinity of the minimum at about 0.042.

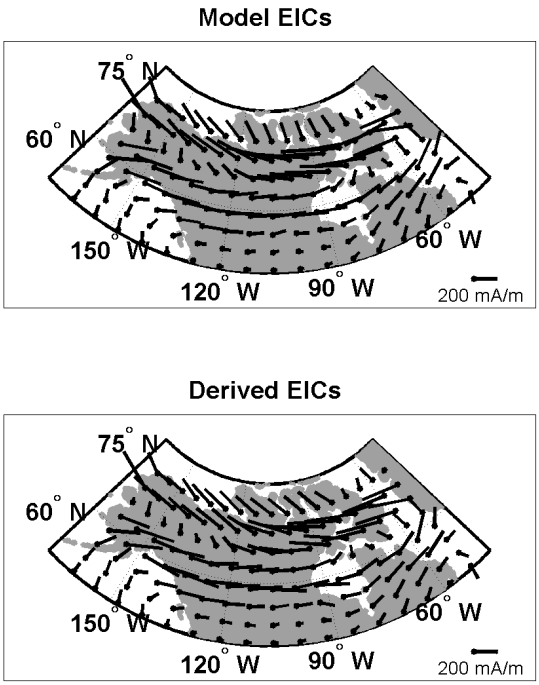

Figure 4a. (top) The model equivalent ionospheric currents and (bottom) the derived equivalent ionospheric currents. The length of the vector indicates the magnitude of the current. This plot shows from 50° GLat to 78° GLat to better display the minor differences between the model and derived currents.

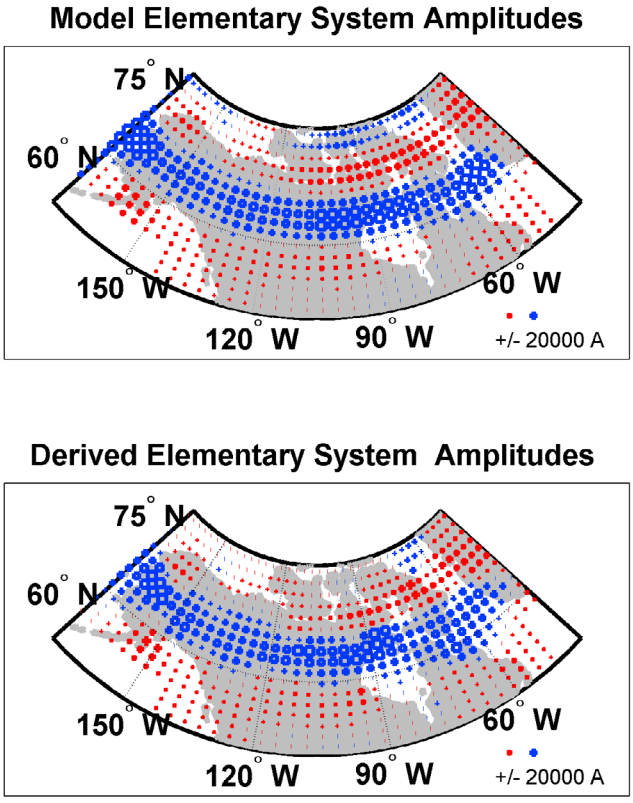

Figure 4b. (top) The model elementary current amplitudes and (bottom) the derived elementary current amplitudes. Red plus symbols indicated downward currents, which are the positive directions for the model, and blue squares indicate upward currents. The size of the symbol indicates the magnitude of the current. The geographic latitudinal and longitudinal ranges of Figure 4b are the same as Figure 4a.

from eastward at about 60° latitude to westward at about 67° latitude. A scale for the horizontal magnetic field magnitude is in the lower right corner of the plot. These model derived magnetic field data were then inverted with the SECS method to determine if the model ionospheric current pattern could be reconstructed with high enough fidelity. Figures 4a and 4b (top) show the model equivalent ionospheric currents and model elementary current amplitudes, respectively. The plus symbols and boxes in Figure 4b indicate positive and negative elementary current poles, respectively, where a pole is defined as the location at which elementary current is derived. The size of the symbol indicates the magnitude of the current pole. In Figure 4a the length of the vector indicates the magnitude of the model ionospheric current and a key for the symbols is present in the lower right corner of the plots. Figures 4a and 4b (bottom) display the model and reconstructed horizontal EICs and EIC amplitudes, respectively, using the spherical elementary current system method. A qualitative comparison of model and derived currents in Figures 4a and 4b show that there is minimal difference between the two current patterns.

[10] For a more quantitative comparison between the model and the SECS output, Figure 5 shows two histograms of the absolute difference between the equivalent ionospheric Jx and Jy components. The mean and median difference in Jx is 3 mA/m with a standard deviation of 16 mA/m. The mean difference in Jy is 4 mA/m and the median is 6 mA/m with a standard deviation of 24 mA/m. Compared to the mean Jx and Jy values the median percentage difference is on the order of 3%. We interpret these differences to mean that we can

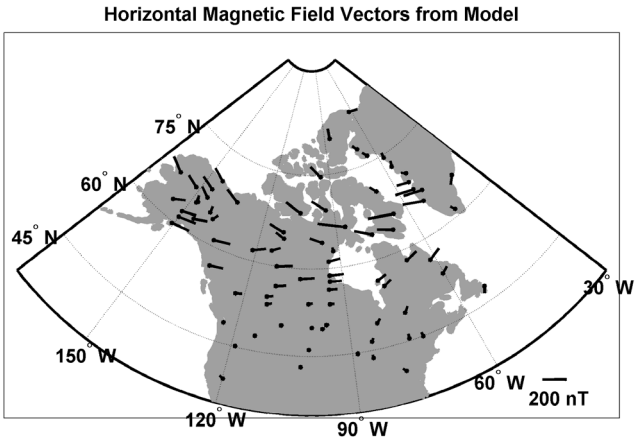

Figure 4c. Horizontal magnetic field vectors derived at the location of the available ground magnetometers from the model ionospheric current system.

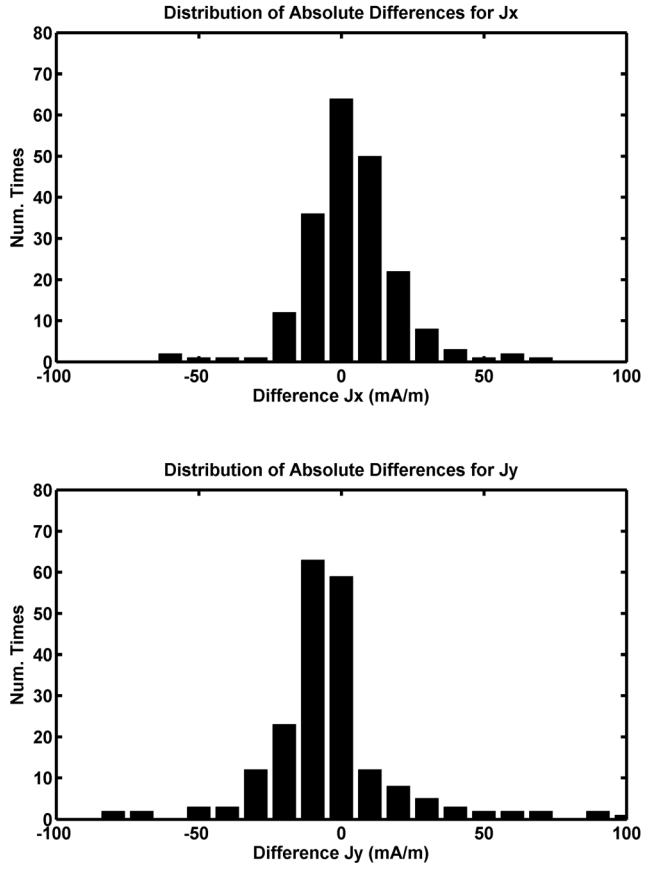

Figure 5. Histograms of the absolute difference between the model ionospheric currents and the derived equivalent ionospheric currents for each component.

reliably reproduce the synthetic ionospheric current systems from the synthetic magnetometer data using the SECS technique.

3.2. The 10 December 2007 Harang Discontinuity

[11] In this section we apply the SECS technique to a real data case of a Harang discontinuity observed over North America at 0647 UT on 10 December 2007. We apply the SECS technique to a real case of a Harang discontinuity as a means of comparing observations with the model case validated in section 3.1 and because it is a large structure in latitude and longitude that is frequently observed during most levels of geomagnetic activity in the nightside sector when the auroral oval is in approximately the latitudinal center of the North American arrays. During this event ground magnetometer data are available from 43 stations. For each of these stations the quiet time background is calculated using quiet ground magnetometer data from December 2007 as well as the month before and the month after. To calculate the quiet time background, intervals of relatively smooth magnetometer data (varying in length from an hour to a whole day) are selected by eye from the Bx and By components for nearly every day over a three month period. These intervals are then averaged together and smoothed to create one 24 h quiet time background interval. Three months of quiet time data are used because it is difficult to obtain a quiet time background from the higher−latitude stations where geomagnetic activity is frequently present. We define quiet data as an interval varying from 1 to 24 h with a low standard deviation in the magnetic field fluctuations and little to no sharp gradients in the magnetic field components. For stations at low latitudes the standard deviation is on the order of 5 to 10 nT, but at higher latitudes the standard deviation is allowed to be as large as 40 nT. We find that the average of the quietest 5 days of each month to be inadequate at the auroral latitudes due to reoccurring geomagnetic activity in the nighttime sector. A comparison of the average of the quietest 5 days and our technique shows that difference on the order of 10 to 20 nT is possible. These differences can have a significant impact on the determination of the equivalent ionospheric currents. Figure 6 shows the corresponding equivalent ionospheric currents, and Figure 7 displays the SECS elementary system amplitudes (scaling factors) for 0647 UT on 10 December 2007.

[12] In Figure 6 the equivalent ionospheric currents for the same time show an eastward current from Alaska to local midnight where it appears to be diverted equatorward by a westward equivalent current that extends from southern Greenland to local midnight and then poleward of the eastward equivalent current. This eastward and westward arrangement of the equivalent ionospheric currents looks similar to the eastward and westward electrojet system at about 75° geographic west longitude in Figure 4a. This configuration of equivalent ionospheric currents is also what we expect for a Harang discontinuity. Since the Harang discontinuity is the location of the ionospheric shear in the flow and the Hall currents are antiparallel to the flow we also expect to see a shear in the equivalent ionospheric currents.

[13] In Figure 6 there are regions within the analysis area we are considering for the SECS that have little or no magnetometer coverage such the James Bay (at about 53° N GLat, 80° W Glong) and the Great Bear Lake (at about 66° N GLat, 121° W Glong) regions in Canada. Some of the regions are

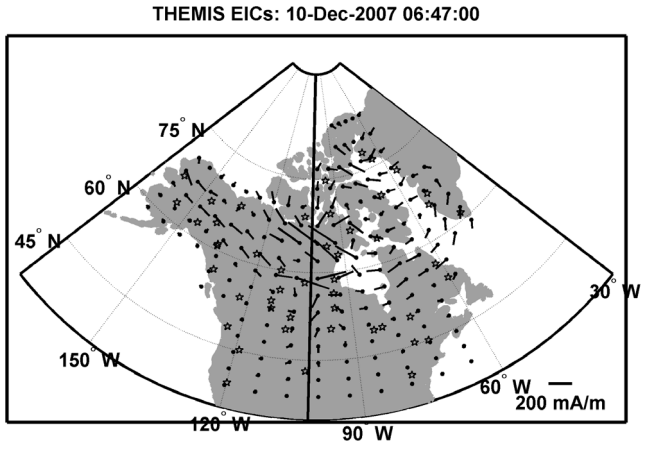

Figure 6. Equivalent ionospheric currents for the Harang discontinuity observed over North America on 10 December 2007 at 0647 UT. The key for the equivalent ionospheric currents is in the lower right corner, and the black line at about 100° geographic longitude is the location of local midnight. The stars mark the location of stations that had ground magnetometer data for that day.

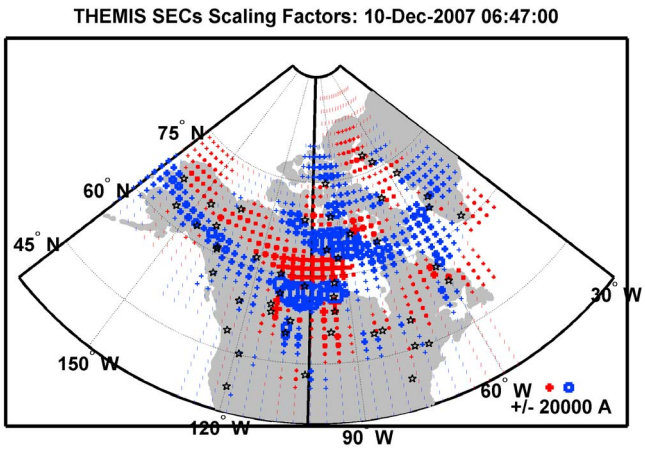

Figure 7. SECS for the Harang discontinuity observed over North America on 10 December 2007 at 0647 UT. The key for the SECS is in the lower right corner, and the black line at about 100° geographic longitude is the location of local midnight. The stars mark the location of stations that had ground magnetometer for that day.

on the order of the size of the area between the Western and Eastern parts of the Greenland array where we have not calculated the equivalent ionospheric currents even though there are magnetometers on the Eastern part of Greenland. However, the James Bay and the Great Bear Lake regions have been included in this study because they are surrounded by a number of ground magnetometer stations that can be used to relatively reliably determine the SECS whereas the center of Greenland is not well bounded by ground magnetometers. *Pulkkinen et al.* [2003] have found that the SECs in low coverage areas are accurate to 15% and as high as 1% when the equivalent ionospheric currents are determined in the region of the ground magnetometers.

[14] If we assume that there are no conductance gradients perpendicular to the electric field direction in the ionosphere, then SECS elementary amplitudes are directly proportional to the FACs. For a detailed discussion on this assumption see *Amm et al.* [2002]. Using this assumption, in Figure 7 we see a strip of downward currents (colored blue) starting on the western side of the analysis area at about 65° geographic latitude and extending to about 57° geographic latitude at 90° geographic west longitude. These downward FACs are similar in appearance to region 2 currents. Just north of the blue FACs is the strip of red FACs that could be associated with the region 1 currents. At about 90° geographic west longitude we see the start of a band of blue downward FACs at about 67° geographic latitude and stretching eastward to the end of the analysis area. Equatorward of that eastern strip of downward FACs is a weak band of upward FACs. This arrangement of alternating down-up-down FACs along the meridian at local midnight, which is marked with the solid black line at about 102° geographic west longitude, is very similar to our model ionospheric currents in Figure 4b at about 100° geographic west longitude and again the arrangement we expect for a Harang discontinuity. The Harang discontinuity is associated with a strong shear in the flow corresponding to a convergent electric field where an upward FAC is observed. Just poleward and equatorward of these upward field aligned currents are the downward region 1 and region 2 currents, respectively, associated with the poleward and equatorward edge of the auroral oval.

[15] Finally, Figure 8 shows a sequence of equivalent ionospheric currents for analysis areas given every 10 min. Figure 8 demonstrates the dynamic changes in the equivalent

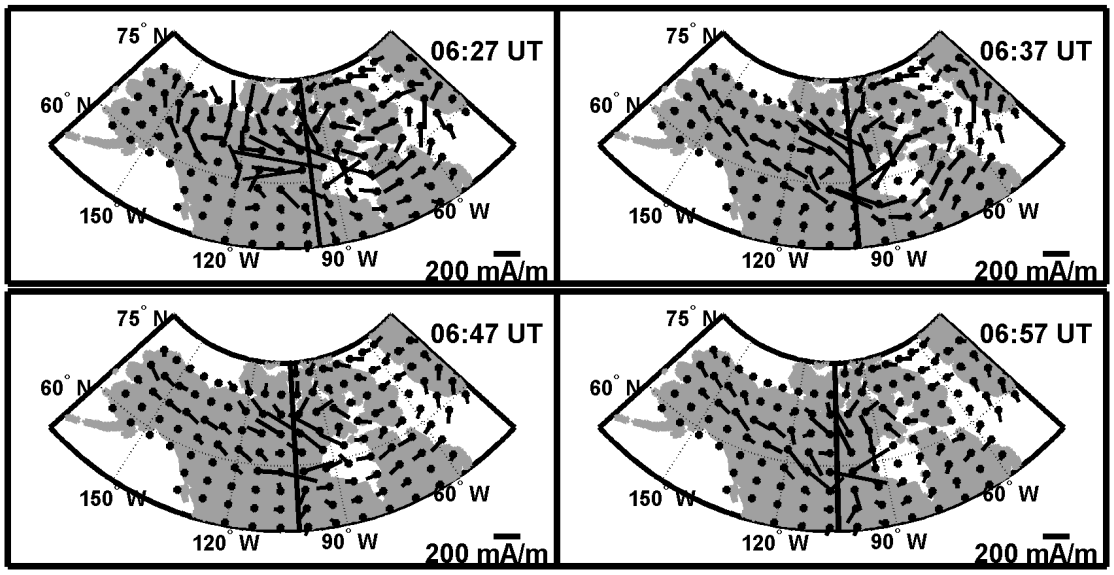

Figure 8. A sequence equivalent of ionospheric currents observed over North America on 10 December 2007 starting at 0627 UT. The key for the equivalent ionospheric currents is in the lower right corner, and the black line at about 100° geographic longitude is the location of local midnight. This sequence demonstrates the dynamics in the equivalent ionospheric currents observed at the end of a geomagnetically active period.

ionospheric currents at the end of a geomagnetically active period where the westward equivalent current weakens between 0627 UT to 0637 UT and organizes into a clear Harang discontinuity at 0647 UT (i.e., the Harang discontinuity shown in Figures 6 and 7). At 0657 UT the equivalent ionospheric currents weaken further and begin to become more disorganized.

4. Summary and Conclusions

[16] By applying the known and widely used technique of SECS [*Amm and Viljanen*, 1999] for determining elementary current amplitudes and equivalent ionospheric currents to the magnetometer arrays in North America and Western Greenland we are able to reproduce model equivalent ionospheric currents of a model Harang discontinuity that are accurate to within a few percent. We then applied the same method to the ground magnetometer data measured in and around a Harang discontinuity and obtained elementary current amplitudes and equivalent ionospheric currents that closely resembled the model Harang currents.

[17] Now that ground magnetometer data are readily available over the Internet ionospheric equivalent currents can be produced on a regular basis for the space physics community using the SECS technique. These currents are extremely valuable for magnetosphere-ionosphere coupling studies especially in conjunction with ionospheric radar measurements, all-sky images, and conjugate spacecraft measurements. For example the equivalent ionospheric currents can contribute physical insights to the topics of substorms, pseudo breakups, and polarward boundary intensifications. During substorm events the cross tail current is diverted through the ionosphere along field aligned currents. The equivalent ionospheric currents provide a picture of the ionosphere during substorms and under the right conditions show the width and length of the ionospheric leg of the substorm current wedge. We have already observed a number of ionospheric portions of substorm current wedges within the equivalent ionospheric currents and the evolution of those wedges throughout the entire substorm. With good magnetic field line models this ionospheric portion of the wedge could be mapped back into the magnetotail to better demonstrate which regions of the magnetotail are involved in the substorm process. In addition, it has been suggested that substorm, pseudo breakups, and poleward boundary intensifications have the same underlying physical mechanism, but occur in different regions of the magnetotail as well as the auroral oval. It has also been theorized that auroral substorm onsets occur within the Harang discontinuity [*Lyons et al.*, 2003]. *Weygand et al.* [2008] and *Zou et al.* [2009] have generally shown this to be true, but no one has investigated whether poleward boundary intensifications and pseudo breakups also occur near the Harang discontinuity like auroral substorm onsets. This topic could be more easily investigated with equivalent ionospheric currents because ionospheric radar measurements are not as plentiful as the grounds magnetometer measurements and the radar measurements have a lower cadence. The temporal resolution of the SECS method is limited only by the resolution of the magnetometers which have a temporal resolution on the order of seconds and a spatial resolution on the order of about 350 km in the case of the North American networks. While the spatial resolution is fairly coarse, the temporal resolution is significantly better than that of radar measurements and on the order of or better than all-sky image measurements. In contrast to radars and all-sky cameras, which can make observations only under favorable weather or geomagnetic circumstances, the equivalent ionospheric currents can be derived from the ground magnetometer data on a nearly continuous basis.

[18] **Acknowledgments.** This work was supported by NASA THEMIS grant SA3650 at UCLA. We would like to thank Martin Conners, Kirsti Kauristie, Robert McPherron, Krishan Khurana, Margaret Kivelson, and Raymond Walker for their helpful discussions. We would also like to thank Hima Gudipati and Bijan Beheshti for their summer work on this study. Some data have been provided by the Geophysical Institute Magnetometer Array operated by the Geophysical Institute, University of Alaska. More information about this data set is available at http://magnet.asf.alaska.edu/. The MACCS magnetometer array is supported through National Science Foundation grant AGS0827903 at Augsburg College. CANMOS data were obtained by the Canadian Magnetic Observatory Network (CANMON), maintained and operated by the Geological Survey of Canada, provided the data used in this study (http://gsc.nrcan.gc.ca/geomag).

[19] Robert Lysak thanks Tohru Araki and another reviewer for their assistance in evaluating this paper.

References

Amm, O. (1997), Ionospheric elementary current systems in spherical coordinates and their application, *J. Geomag. Geoelectr.*, *49*, 947–955.

Amm, O. (1998), Method of characteristics in spherical geometry applied to a Harang discontinuity situation, *Ann. Geophys.*, *16*, 413–424, doi:10.1007/s00585-998-0413-2.

Amm, O., and A. Viljanen (1999), Ionospheric disturbance magnetic field continuation from the ground to the ionosphere using spherical elementary currents systems, *Earth Planets Space*, *51*, 431–440.

Amm, O., M. J. Engebretson, T. Hughes, L. Newitt, A. Viljanen, and J. Waterman (2002), A traveling convection vortex event study: Instantaneous ionospheric equivalent currents, estimation of field−aligned currents, and the role of induced currents, *J. Geophys. Res.*, *107*(A11), 1334, doi:10.1029/2002JA009472.

Chapman, S., and J. Bartels (1940), Geomagnetism, vol. 2, Oxford Univ. Press, London.

Engebretson, M. J., W. J. Hughes, J. L. Alford, E. Zesta, L. J. Cahill Jr., R. L. Arnoldy, and G. D. Reeves (1995), Magnetometer array for cusp and cleft studies observations of the spatial extent of broadband ULF magnetic pulsations at cusp/cleft latitudes, *J. Geophys. Res.*, *100*, 19,371–19,386, doi:10.1029/95JA00768.

Haines, G. V. (1985a), Spherical cap harmonic analysis of geomagnetic secular variation over Canada 1960–1983, *J. Geophys. Res.*, *90*, 12,563–12,574, doi:10.1029/JB090iB14p12563.

Haines, G. V. (1985b), Spherical cap harmonic analysis, *J. Geophys. Res.*, *90*, 2583–2591, doi:10.1029/JB090iB03p02583.

Lyons, L. R., C.-P. Wang, and T. Nagai (2003), Substorm onset by plasma sheet divergence, *J. Geophys. Res.*, *108*(A12), 1427, doi:10.1029/2003JA010178.

Mersmann, U., W. Baumjohann, F. Küppers, and K. Lange (1979), Analysis of an eastward electrojet by means of upward continuation of ground−based magnetometer data, *J. Geophys.*, *45*, 281–298.

Press, W. H., B. P. Flannery, S. A. Teukolsky, and W. T. Vetterling (1992), Singular value decomposition, in *Numerical Recipes in FORTRAN: The Art of Scientific Computing*, 2nd ed., pp. 51–63, Cambridge Univ. Press, Cambridge, U. K.

Pulkkinen, A., O. Amm, and A. Viljanen (2003), Ionospheric equivalent current distributions determined with the method of spherical elementary current systems, *J. Geophys. Res.*, *108*(A2), 1053, doi:10.1029/2001JA005085.

Untiedt, J., and W. Baumjohann (1993), Studies of polar current systems using the IMS Scandinavian magnetometer array, *Space Sci. Rev.*, *63*, 245–390, doi:10.1007/BF00750770.

Weygand, J. M., R. L. McPherron, H. Frey, O. Amm, K. Kauristie, A. Viljanen, and A. Koistinen (2008), Relation of substorm onset to Harang discontinuity, *J. Geophys. Res.*, *113*, A04213, doi:10.1029/2007JA012537

Zou, S., L. R. Lyons, C. -P. Wang, A. Boudouridis, J. M. Ruohoniemi, P. C. Anderson, P. L. Dyson, and J. C. Devlin (2009), On the coupling between the Harang reversal evolution and substorm dynamics: A syn-

thesis of SuperDARN, DMSP, and IMAGE observations, *J. Geophys. Res.*, *114*, A01205, doi:10.1029/2008JA013449.

O. Amm and A. Viljanen, Arctic Research Unit, Finnish Meteorological Institute, PO Box 503, FI-00101 Helsinki, Finland.

V. Angelopoulos and J. M. Weygand, Institute of Geophysics and Planetary Physics, University of California, 3845 Slichter Hall, 405 Charles E. Young Dr., PO Box 951567, Los Angeles, CA 90095, USA. (jweygand@igpp.ucla.edu)

M. J. Engebretson and D. Murr, Augsburg College, 2211 Riverside Ave. South, Minneapolis, MN 55454, USA.

H. Gleisner, Danish Meteorological Institute, Lyngbyvej 100, Copenhagen DK-2100, Denmark.

I. Mann, Department of Physics, University of Alberta, Edmonton, AB T6G 2J1, Canada.